Chinese Chemical Letters 36 (2025) 110065

Contents lists available at ScienceDirect

Chinese Chemical Letters

journal homepage: www.elsevier.com/locate/cclet

Design of carbon@WS_2 host with graham condenser-like structure for tunable sulfur loading of lithium-sulfur batteries

Yue Wang[a], Wenli Hu[a], Binchao Shi[a], He Jia[b], Shilin Mei[a,c,*], Chang-Jiang Yao[a,*]

[a] State Key Laboratory of Explosion Science and Safety Protection, School of Mechatronical Engineering, Beijing Institute of Technology, Beijing 100081, China
[b] Institute of Condensed Matter and Nanoscience (IMCN), Université catholique de Louvain, Place L. Pasteur, 1, 1348 Louvain-la-Neuve, Belgium
[c] Xi'an Safety Energy Technology Co., Ltd., Xi'an 710299, China

ARTICLE INFO

Article history:
Received 16 March 2024
Revised 27 April 2024
Accepted 27 May 2024
Available online 28 May 2024

Keywords:
Lithium sulfur battery
AAO
Aligned nanotubes
Tunable sulfur loading
WS_2

ABSTRACT

Despite significant progress has been achieved regarding the shuttle-effect of lithium polysulfides, the suppressed specific capacity and retarded redox kinetics under high sulfur loading still threat the actual energy density and power density of lithium-sulfur batteries. In this study, a graham condenser-inspired carbon@WS_2 host with coil-in-tube structure was designed and synthesized using anodic aluminum oxide (AAO) membrane with vertically aligned nanopores as template. The vertical array of carbon nanotubes with internal carbon coils not only leads to efficient charge transfer across through the thickness of the cathode, but also provides significant confinement to polysulfide diffusion towards both the lateral and longitudinal directions. Few-layer WS_2 in the carbon coils perform a synergistic role in suppressing the shuttle-effect as well as boosting the cathodic kinetics. As a result, high specific capacity (1180 mAh/g at 0.1 C) and long-cycling stability at 0.5 C for 500 cycles has been achieved at 3 mg_S/cm^2. Impressive areal capacity of 7.4 mAh/cm^2 has been demonstrated when the sulfur loading reaches 8.4 mg/cm^2. The unique coil-in-tube structure developed in this work provides a new solution for high sulfur loading cathode towards practical lithium-sulfur batteries.

On pursuing future energy storage systems (ESSs) with high output performances and sustainability, a series of new ESSs beyond lithium-ion batteries (LIBs) have attracted growing attention due to the bottle-neck of LIBs towards higher energy/power density [1-3]. As one of the most promising candidates for the next-generation ESSs, lithium-sulfur (Li-S) batteries outperform others due to the low cost of nature abundant sulfur and high theoretical capacity (1675 mAh/g). Up to date, significant progresses have been achieved regarding the notorious problems that hinder the practical application of Li-S batteries, such as the "shuttle effect" of lithium polysulfides in state-of-the-art ether-based electrolytes, the sluggish kinetics due to the insulating nature of sulfur species, and the destructive volume expansion of the lithiated cathode [4-7]. Numerous cathodes involving advanced catalysis and well-defined structures have been developed to realize high performance even with lean electrolyte [8-13]. With respect to prototype Li-S batteries, high capacity, high energy density, and acceptable power density are undoubtedly necessary to adopt their practical use, which requires a high mass loading of the active material [14-16]. However, in pouch cells with high-loading-cathodes, achieving fast kinetics remains a long-standing challenge since the aforementioned problems are even more sever in these thick electrodes. Specifically, the reaction kinetics is even more sluggish due to the proportional increase in the electron- and ion transport distance. Moreover, on account of the increased sulfur concentration gradient in the high-loading-cathode, the shuttle-effect tends to be intensified, leading to sever capacity decay during cycling. Besides, increasing areal loading usually leads to new challenges such as fracturing and delamination of the thick electrodes. In principle, building long-range conducting paths for efficient electron and ion transfer has been the most straightforward approach to eliminate the retarded kinetics and improve the stability of thick electrodes, thus to realize comparable electrochemical performances to that under low sulfur loading [14].

Among various sulfur host materials, low-tortuous arrays featuring both short and continuous electron- and ionic conducting paths have been demonstrated beneficial to achieving high-rate and prolonged cycling life of lithium batteries [17-21]. Besides facilitated mass transport, strong confinement and fast conversion of polysulfides are additional preset for sulfur cathode for practical application. In this regard, one-dimensional nanostructures such as hollow carbon nanotube (CNT) stand out from many

* Corresponding authors.
E-mail addresses: shilin.mei@bit.edu.cn (S. Mei), cjyao@bit.edu.cn (C.-J. Yao).

https://doi.org/10.1016/j.cclet.2024.110065
1001-8417/

other structures due to their straight conducting route and tubular space for encapsulating and confining of sulfur species [22,23]. In addition, strong interactions between the nonpolar carbon and the polar Li_2S can be introduced by surface modification of amphiphilic organic molecules on the inner carbon wall to further constrain the sulfur species. Although more complicated structures were reported afterwards such as small CNT embedded micro carbon tubes and spheres-in-tube structures [24,25], the rational design of one-dimensional sulfur host still needs systematic study to realized optimized output performances under high areal loading of sulfur.

Motivated by the aforementioned research, a multifunctional C@WS_2 host with coil-in-tube structure inspired by the Graham condenser was designed in purpose to induce rapid electron and ion transfer, tunable sulfur loading, strong confinement and fast conversion of polysulfide species. The one-dimensional carbon nanotubes with internal carbon coils allow efficient charge transfer across through the thickness of the cathode and provide strong physical confinement to polysulfide diffusion towards both the lateral and longitudinal directions. The Few-layer WS_2 loaded in the carbon coils provides additional adsorption sites for polysulfides, performing a synergistic role in suppressing the shuttle-effect and boosting the cathodic kinetics.

Nanoporous AAO membrane (200 nm in diameter) with vertically aligned nanochannels and block copolymer of polystyrene-*b*-poly(2-vinylpyridine) (PS-*b*-P2VP) are used as hard and soft template, respectively. The inner coil is induced by PS-*b*-P2VP, which forms helix micelles inside the AAO channels driven by the confined phase separation [26]. As shown in Fig. S1 (Supporting information), PS-*b*-P2VP/THF+DMF solution was firstly filled into the AAO channels *via* drop wetting and subsequently immersed into water to induce a fast phase separation. Helix micelles were generated due to the microphase separation under the spatial confinement of AAO nanochannels driven by the fast extraction of THF+DMF from PS-*b*-P2VP into water. The total molecular weight which determines the micelle size and the volume ratio of PS:P2VP that presents its hydrophilic property are found to be crucial in the formation of helix coils. PS_{50000}-*b*-$P2VP_{16500}$ with a volume ratio of PS:P2VP = 3.03 was demonstrated adoptable for the fabrication of helix coils under the confinement of 200 nm nanochannels, while those with larger or smaller PS content would form disordered structures due to the weaker or stronger interactions between the hydrophilic P2VP and water. In order to transform the PS-*b*-P2VP micelles into carbon nanotubes, polydopamine (PDA) was applied as carbon source and uniformly coated on the surface of PS-*b*-P2VP as well as the inner wall of AAO channels (Fig. 1a, step 1). WS_2 nanodomains are generated by the adsorption of WS_4^{2-} ions and the subsequent decomposition under acid conditions (pH~3) (Fig. 1a, step 2). Finally, the PS-*b*-P2VP template was removed by a thermal annealing process and carbon tubes with helix coils inside can be obtained. The prepared C@WS_2 host was filled with sulfur and used as cathode in the subsequent process (Fig. 1a, step 3).

Figs. 1b and c show the morphology change of the AAO membrane before and after filling with the C@WS_2 tubes, in which the color changes from white to black. Fig. 1d shows the thickness of the AAO membrane is about 60 μm, which is filled with PS-*b*-P2VP helix coils (Figs. 1e–g) inside the channels. EDS mapping of the C@WS_2 tubes inside the AAO membrane show homogeneous distribution of S, C, N, W elements, which were derived from the carbonized PDA and incorporated WS_2 (Fig. 1h). TEM image further confirms the replica of the PS-*b*-P2VP template by PDA, showing the well-defined coil-in-tube structure after carbonization (Fig. 1i). High-resolution TEM (HRTEM) image reveals the formation of few-layer WS_2 inside the amorphous carbon where crystal domains with an adjacent lattice fringe of 0.62, 0.27, 0.16, and 0.26 nm corresponding to the (002), (100), (101) and (110) plane of WS_2 can

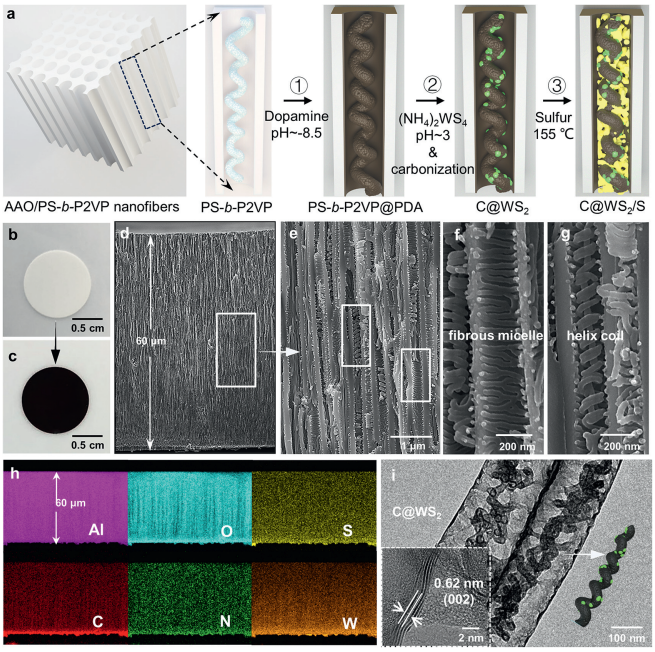

Fig. 1. (a) Schematic illustration of the fabrication process for the C@WS_2 composites. (b, c) SEM images of AAO and AAO-C@WS_2 surfaces. (d-g) SEM images of PS-*b*-P2VP coils inside the AAO channels. (h) EDS mapping of the cross-section view of the AAO-C@WS_2 membrane. (i) TEM image of the C@WS_2 coil-in-tube structures. Inset: HRTEM image of the WS_2 domains.

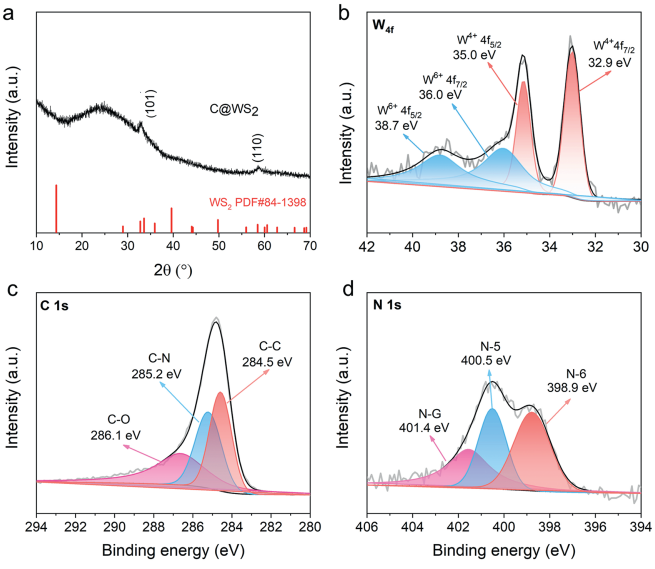

Fig. 2. (a) XRD pattern and high-resolution XPS spectrum of (b) W 4f, (c) C 1s, and (d) N 1s for the C@WS_2 composites.

be found, suggesting the successful loading of WS_2 (Fig. S2 in Supporting information).

XRD pattern of the C@WS_2 host is shown in Fig. 2a. Sharp reflexes at 2θ of 33.6° and 58.4° corresponding to the 101 and 110 plane of WS_2 are observed (PDF No. 84-1398) [27,28]. In addition, a broad peak centered at 24.8° can be indexed to the amorphous phase-dominated carbon derived from PDA. In XPS spectra, the W 4f spectrum (Fig. 2b) [29-33] is fitted by three characteristic peaks of W^{4+}, ascribed to W $4f_{7/2}$ (32.9 eV) W $4f_{5/2}$ (35.0 eV). Besides, the peaks at 36.0 and 38.7 eV are assigned to W $4f_{7/2}$, W $4f_{5/2}$ of W^{6+}, respectively, which can be attributed to a slight oxidation of the WS_2 surface. In the S 2p [34-36] spectrum (Fig. S3 in Sup-

porting information), the peaks at 162.5 and 163.3 eV belong to S $2p_{3/2}$, S $2p_{1/2}$ of sulfidic nature. The splitting signals positioned at approximately 164.3 and 165.6 eV are assigned to the C–S–C bond, which is derived from the interaction between PDA and WS_4^{2-} during the synthetic process of WS_2. In the C 1s spectrum (Fig. 2c), peaks at 284.5 and 286.1 eV correspond to the C–C and C–O bonds, respectively. The existing of C-N bond at 285.2 eV indicates the generation of N-doped carbon from PDA. The N 1s [37,38] spectrum in Fig. 2d shows three peaks at 398.9, 400.5, and 401.4 eV, which can be ascribed to three nitrogen's chemical states, namely the pyridinic N (N-6), pyrrolic N (N-5), and graphitic N (N-G), respectively. The N-doped carbon not only can provide additional polar sites to adsorb polysulfides, but also can accelerate the redox reaction *via* efficient electron transfer of graphitic N.

The S/C@WS_2 cathode was prepared by the melting-infusion method at 155 °C with different areal loading of sulfur and assembled into Li-S coin cells with 100 μm lithium foil as the anode. TEM image shows that the melt sulfur was successfully filled inside the tubular structure (Fig. S4 in Supporting information). The cathode kinetics is systematically analyzed to evaluate the functions of the designed C@WS_2 host with coil-in-tube structure. Carbon nanotubes (CTs) generated from AAO without coils and WS_2 nanocatalyst were applied for comparison. The galvanostatic intermittent titration technique (GITT) is adopted to decouple the total cathodic polarization (η_{total}) during discharge into activation polarization (η_{ac}), concentration polarization (η_{con}), and ohmic polarization (η_{ohm}) [39]. Specifically, the sum of η_{ohm} and η_{ac} can be indicated by the instantaneous voltage jump at the end of the discharge step, and the η_{con} can be represented by the following voltage recovery to the equilibrium voltage in the relaxation stage. As shown in Figs. 3a–c, the decoupled η_{total} at the Li_2S nucleation stage (depth of discharge between 27% and 70%, Fig. S5 in Supporting information) is compared between the C@WS_2 and CTs host. C@WS_2 host with WS_2 nanocatalyst and coil-in-tube structure show smaller $\eta_{ohm}+\eta_{ac}$ and η_{con}, suggesting that the C@WS_2 host shall significantly reduce the polarization required for interfacial charge transfer determined by the activation energy of electrode reaction (η_{ac}) and ohmic resistance of electrolyte under a certain current (η_{ohm}), as well as the concentration polarization caused by the concentration differences of the reaction species between the electrode surface and the bulk electrolyte (η_{con}). In addition, the Li_2S precipitation test with constant potential discharge at 2.05 V *vs.* Li/Li^+ is performed to validate the catalytic performance of the C@WS_2 host [40-43]. As shown in Fig. 3d and Fig. S6 (Supporting information), the C@WS_2 host exhibits clear response of Li_2S nucleation (at 6450 s), while the CTs reference shows no obvious Li_2S nucleation peak, indicating efficient electrocatalytic activity of WS_2 towards lithium polysulfides. According to Faraday's law, the Li_2S precipitation capacitiy of C@WS_2 based cathode is 294.4 mAh/g, which is higher than that of CTs based cathode (59.19 mAh/g), implying more conversion of lithium polysulfides to Li_2S. Therefore, C@WS_2 not only promotes the initial nucleation but also guides the subsequent deposition of Li_2S, showing a favorable catalytic effect on the redox reaction owing to the highly active sites of few-layer WS_2. Further evaluation on the Li_2S growth behavior is conducted using the classical Scharifer-Hills (SH) and Bewick-Fleischman-Thirsk (BFT) models to fit the curves of current *vs.* time in the potentiostatic discharging process (Fig. 3e). The fitted result shows that the Li_2S growth on the C@WS_2 host matches better with the 2DI nucleation model, suggesting the Li_2S growth rate will be controlled by lattice bonding, which can be attributed to the existence of sulfurphilic WS_2.

The electrochemical properties of the S/C@WS_2 electrode were further revealed by CV measurements under various scan rates ranging from 0.02 mV/s to 0.1 mV/s (Fig. S7 in Supporting information). The C@WS_2 cell exhibits two typically cathodic peaks at

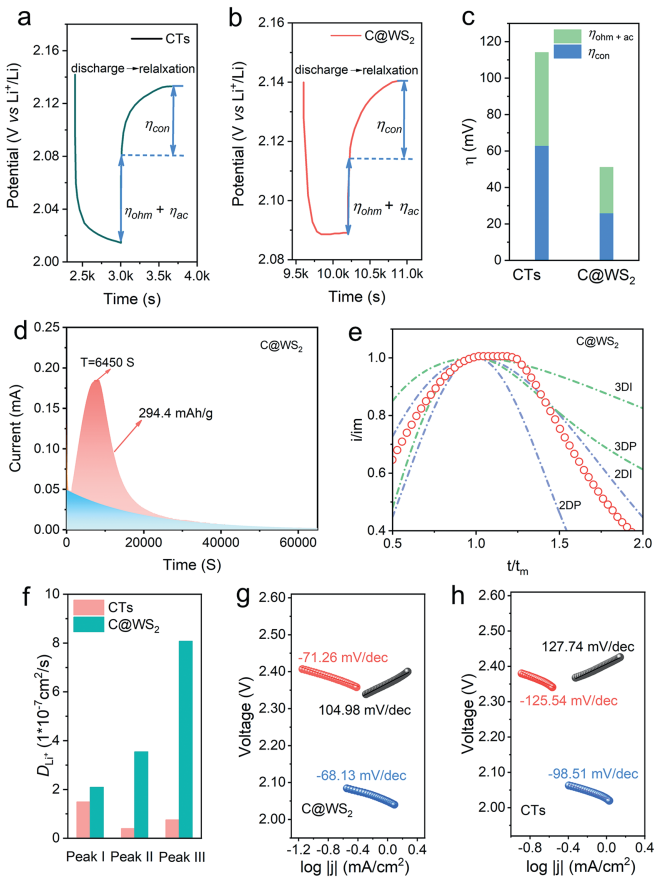

Fig. 3. (a, b) Decoupled total cathodic polarization (η_{total}) of the S/C@WS_2 and S/CTs batteries based on the GITT measurements. (c) Polarization analysis at the Li_2S nucleation stage. (d) Current-time plots of catholyte Li_2S_8 on the S/C@WS_2 cathodes potentiostatically discharged at 2.06 V. (e) The dimensionless transient of Li_2S deposition in comparison with theoretical 3D and 2D electroplating models (*t*: time, t_m: time needed to reach the maximum current; *i*: current, i_m: maximum current). (f) Lithium-ion diffusion rate and (g, h) tafel plots of different cathodes.

about 2.3 V and 1.93 V and two closed (merged) anodic peaks at around 2.4 V corresponds to the reversible sulfur redox reactions (Figs. S7a and b). Li^+ diffusion coefficients (D_{Li^+}) can be calculated by the classical Randles-Sevcik equation ($i_p = 2.69\times10^5\times A\times z^{1.5}\times D_{Li^+}^{0.5}\times\nu^{0.5}\times C_{Li^+}$), where i_p is the peak current measured in the CV curve, *z* is the number of transferred charges, *A* is the area of the electrode, ν is the scanning rate, C_{Li^+} is the concentration of Li^+ in the electrolyte. The linear fitting relations of $i_p/\nu^{0.5}$ of the two sulfur cathodes are shown in Figs. S7c and d and the D_{Li^+} is summarized in Fig. 3f. In comparison with the CTs host, the S/C@WS_2 exhibits greatly improved Li^+ transfer in the cell. Moreover, the kinetics in liquid-solid reaction and solid-liquid reaction is further verified by the Tafel slope derived from CV curve (Fig. S8 in Supporting information). As shown in Figs. 3g and h, the S/C@WS_2 cathode shows smaller Tafel slope for all the three redox peaks, indicating better bidirectional catalysis of C@WS_2 than that of CTs.

Fig. 4a shows the galvanostatic charge/discharge profiles of the S/C@WS_2 cathode, from which small voltage hysteresis ($\Delta E = 0.14$ V) can be observed, corresponding to small electrochemical polarization. Electrochemical impedance spectroscopy (EIS) is used to monitor the changes of the inner resistance related to the structure and electrochemical evolution during the cycling. Compared to the initial state before cycling, the charge transfer resistance (R_{ct}) and Warburg impedance of the S/C@WS_2 battery greatly decrease after 5 cycles due to the redistribution of sulfur species after the

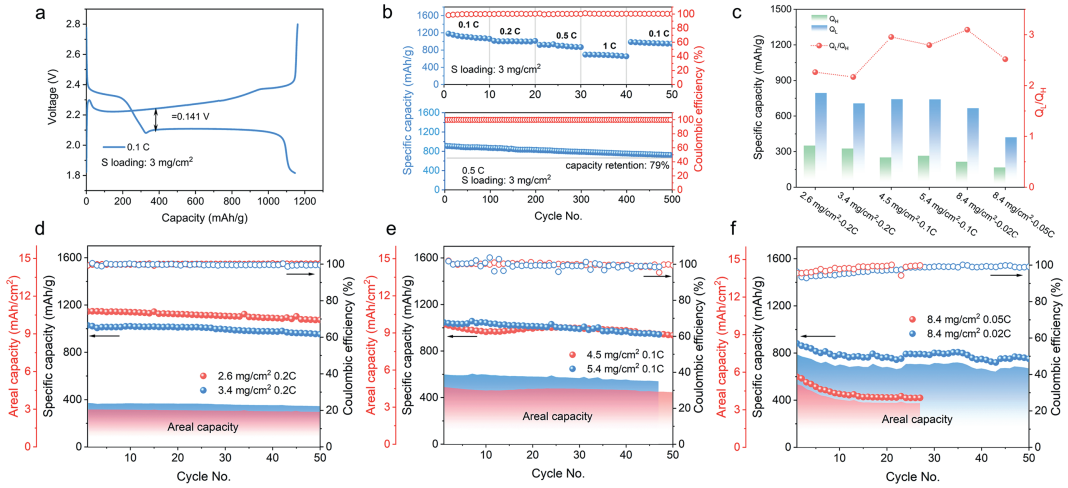

Fig. 4. (a) Charge/discharge profile of the S/C@WS_2 battery at 0.1 C. (b) Rate performance and cycling performance at 0.5 C. (c) Capacity contributions of Q_L and Q_H of the batteries with different sulfur loading at different C rates. (d-f) Cycling performance and the corresponding areal capacity of the batteries different sulfur loading at different C rates.

activation process. In the subsequent cycles the impedance stable, suggesting good reversibility of the redox reactions (Fig. S9 in Supporting information). Fig. 4b illustrates the cycling performances of the S/C@WS_2 battery at moderate sulfur loading of approximately 3 mg/cm^2 under different C rates. Reversible specific capacities of 1180, 1014, 920, 695 and 200 mAh/g are obtained at 0.1, 0.2, 0.5, and 1 C, respectively. When the current rate returns to 0.1 C, reversible specific capacity of 986 mAh/g is sustained, which is comparable to the initial state. Long-term cycling of the S/C@WS_2 battery at 0.5 C has been investigated, which shows a high discharge capacity of 900 mAh/g and a remarkable capacity retention of 79% after 500 cycles. Analysis on the capacity contributions (denoted as Q_H and Q_L, corresponding to the conversion of long-chain polysulfides (the higher plateau) and short-chain polysulfides (the lower plateau), respectively) have been conducted for the battery with different sulfur loading. As shown in Fig. 4c, the highest Q_L/Q_H of 3.09 has been achieved with the areal loading of 8.4 mg/cm^2 at 0.02 C, which is quite close to the ideal contribution of the redox conversion from Li_2S_4 to Li_2S (~75% of the total discharge capacity). Another two high Q_L/Q_H values can be observed in the case of 4.5 and 5.4 mg/cm^2 at 0.1 C (2.95 and 2.79, respectively), suggesting that full redox conversion shall be realized under high mass loading with appropriate current density.

In practical applications, the amount of sulfur loading at the cathode is one of the key indicators that determine the actual energy density of Li-S batteries. In previous studies, a low sulfur loading usually helps to improve the specific capacity and cycling stability, but it leads to a dramatic decrease in the overall energy density of the battery. For the sake of further confirming the functionality of the C@WS_2 host, tunable sulfur loading of 2.6, 3.4, 4.5, 5.4 and up to 8.4 mg/cm^2 has been investigated with the E/S ratio of 10 μL/mg$_S$ (Figs. 4d–f). Typical discharge plateau is clearly displayed in the charge/discharge curves at different current densities (Fig. S10 in Supporting information). Notably, the kinetic voltage of the S/C@WS_2 battery shows almost no decrease as the sulfur loading increased to 8.4 mg/cm^2, dictating the smooth electron/ion transfer and efficient catalysis of the C@WS_2 host. As shown in Figs. 4d–f, the initial specific capacity of the batteries reaches 1145 mAh/g for 2.6 mg/cm^2 at 0.2 C, 1028 mAh/g for 3.4 mg/cm^2 at 0.2 C, 1045 mAh/g for 2.6 mg/cm^2 at 0.1 C, 881 mAh/g for 8.4 mg/cm^2 at 0.02 C, corresponding to areal capacity of 3.0, 3.5, 5.6 and 7.4 mg/cm^2, respectively. The coulombic efficiency for different sulfur loading keeps above 98.8%, suggesting good reversibility of the charge-discharge reactions under high sulfur loading.

The excellent electrochemical performances can be attributed to the synergistic effect of the C@WS_2 host with coil-in-tube structure, which not only provides short path for charge transfer, but also strong adsorption to polysulfides and efficient catalysis for the conversion reaction (Fig. 5a). Specifically, the host material serves as efficient conducting framework which enable electron transfer from both the tube wall and the inner coil. The one-dimensional tubular structure shall regulate the ion transfer within a short pathway, which is favorable for fast kinetics. Notably, sulfur species could be seriously constrained inside the Graham condenser-like tubes. During discharging, the lateral diffusion of lithium polysulfides would be prohibited by the carbon tube wall and the longitudinal diffusion shall pass through the inner coil, during which lithium polysulfides would be blocked by the strong adsorption (Fig. S11 in Supporting information) of the WS_2 nanodomains [44] and the N-doped carbon. Simultaneously, the kinetics of soluble polysulfides could be facilitated at the “triple-phase” interface. Fig. 5b shows the diffusion experiment of Li_2S_6 performed with Celgard, AAO-CTs, and AAO-C@WS_2 membranes as filters. The colorless solution on the right side of the chamber after 24 h confirms the significant intercept of polysulfides for the C@WS_2 host, while the two references show very limited intercepting capability. The strong confinement of the coil-in-tube structure to polysulfides is further verified by decomposition of the cycled batteries and the electron probe X-ray microanalysis (EPMA) results of the lithium anode (Figs. 5c and d). The lighter color in the separator and lithium anode of the S/C@WS_2 battery as well as the much less sulfur species on the surface of lithium anode in comparison with that of the S/CTs batteries confirm the mitigated “shuttle effect” by the Graham condenser-like C@WS_2 host.

In summary, we designed and fabricated a novel C@WS_2 host material with coil-in-tube structure inspired by the Graham condenser for tunable loading of sulfur. Due to the advantages of both the novel structure and well-designed chemical components, the cathode material shows good electron-and ionic conductivity, strong adsorption and electrocatalytic ability to lithium polysulfides, which effectively promotes excellent electrochemical performances of Li-S batteries with tunable sulfur loading. Under a moderate sulfur loading of 3 mg/cm^2, the S/C@WS_2 cathode delivers remarkable high specific capacity of 1180 mAh/g at 0.1 C and long-cycling stability with a 79% capacity retention at 0.5 C after 500 cycles. Under high sulfur loading of 8.4 mg/cm^2, impressive areal capacity of 7.4 mAh/cm^2 has been realized at 0.02 C. The synergistic effect derived from the combination of structural and compo-

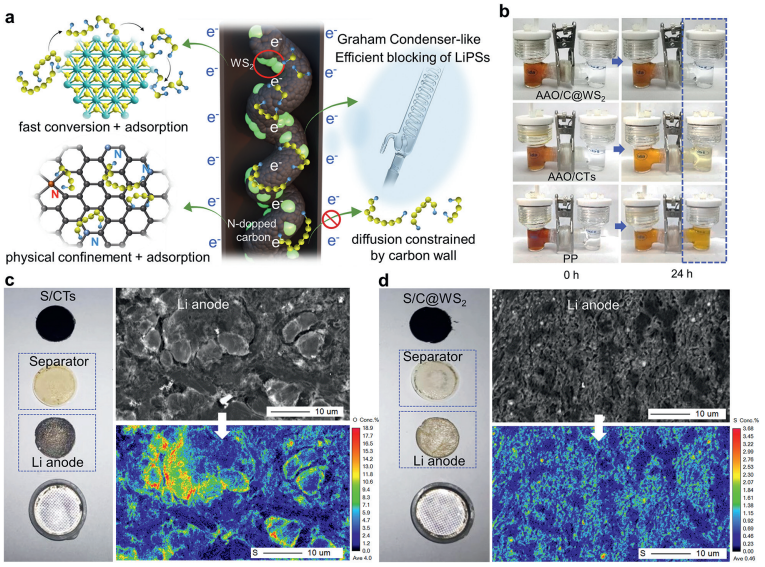

Fig. 5. (a) Schematic illustration of the synergistic effect derived from the C@WS_2 host with coil-in-tube structure. (b) Li_2S_6 permeation experiment in H-shaped glass container with AAO-C@WS_2 separator, AAO-C separator, and Celgard. (c, d) Images of disassembled coin cells using CTs and C@WS_2 as sulfur host and the corresponding SEM images and EPMA mapping of the Li anode.

sitional design propose a new way to tackle the key problems of Li-S batteries on the way towards practical use.

Declaration of competing interest

The authors have no conflicts to declare.

CRediT authorship contribution statement

Yue Wang: Writing – original draft, Investigation, Formal analysis, Data curation. **Wenli Hu:** Visualization, Formal analysis. **Binchao Shi:** Investigation, Data curation. **He Jia:** Methodology, Visualization. **Shilin Mei:** Writing – review & editing, Supervision, Methodology, Conceptualization. **Chang-Jiang Yao:** Writing – review & editing, Project administration, Funding acquisition, Formal analysis.

Acknowledgments

We are grateful to the National Natural Science Foundation of China (Nos. 22075027, 52003030), Starting Grant from Beijing Institute of Technology and financial support from the State Key Laboratory of Explosion Science and Safety Protection (Nos. YBKT21-06, YBKT23-05), and Beijing Institute of Technology Research Fund Program for Young Scholars.

Supplementary materials

Supplementary material associated with this article can be found, in the online version, at doi:10.1016/j.cclet.2024.110065.

References

[1] X. Ji, K.T. Lee, L.F. Nazar, Nat. Mater. 8 (2009) 500–506.
[2] P.G. Bruce, S.A. Freunberger, L.J. Hardwick, J.M. Tarascon, Nat. Mater. 11 (2012) 19–29.
[3] Y.X. Yin, S. Xin, Y.G. Guo, L.J. Wan, Angew. Chem. Int. Ed. 52 (2013) 13186–13200.
[4] W. Sun, Z. Song, Z. Feng, et al., Nano-Micro Lett. 14 (2022) 222.
[5] Z. Ye, Y. Jiang, L. Li, F. Wu, R. Chen, Adv. Mater. 32 (2020) 2002168.
[6] Y. Tian, G. Li, Y. Zhang, et al., Adv. Mater. 32 (2020) 1904876.
[7] Q. Shao, S. Zhu, J. Chen, Nano Res. 16 (2023) 8097–8138.
[8] S. Evers, L.F. Nazar, Acc. Chem. Res. 46 (2013) 1135–1143.
[9] A. Manthiram, Y. Fu, S.H. Chung, C. Zu, Y.S. Su, Chem. Rev. 114 (2014) 11751–11787.
[10] S. Chandra, P. Dutta, K. Biswas, ACS Nano 16 (2022) 7–14.
[11] D. Yang, Z. Liang, C. Zhang, et al., Adv. Energy Mater. 11 (2021) 2101250.
[12] D. Yang, Z. Liang, P. Tang, et al., Adv. Mater. 34 (2022) 2108835.
[13] D. Yang, C. Li, M. Sharma, et al., Energy Storage Mater. 66 (2024) 103240.
[14] M. Wang, Z. Bai, T. Yang, et al., Adv. Energy Mater. 12 (2022) 2201585.
[15] B.Q. Li, Q. Zhang, Sci. China Chem. 64 (2021) 337–338.
[16] J.S. Kim, T.H. Hwang, B.G. Kim, J. Min, J.W. Choi, Adv. Funct. Mater. 24 (2014) 5359–5367.
[17] B. Wang, W. Guo, Y. Fu, ACS Appl. Mater. Interfaces 12 (2020) 5831–5837.
[18] Y. Shi, B. Li, Y. Zhang, et al., Adv. Energy Mater. 11 (2021) 2003663.
[19] K. Huang, P. Zhai, J.S. Chen, et al., Electrochem. Commun. 144-145 (2022) 107395.
[20] Z. Wu, Z. Cai, B. Fang, et al., ACS Appl. Mater. Interfaces 13 (2021) 25890–25897.
[21] S.X. Liu, J.L. Tian, W. Zhang, Nanotechnology 32 (2021) 222001.
[22] G. Zheng, Q. Zhang, J.J. Cha, et al., Nano Lett. 13 (2013) 1265–1270.
[23] Z. Li, B.Y. Guan, J. Zhang, X.W. Lou, Joule 1 (2017) 576–587.
[24] Y. Ge, Z. Chen, S. Ye, et al., J. Mater. Chem. A 6 (2018) 14885–14893.
[25] F. Jin, S. Xiao, L. Lu, Y. Wang, Nano Lett. 16 (2016) 440–447.
[26] P. Hou, H. Fan, Z. Jin, Macromolecules 48 (2015) 272–278.
[27] Y. Liu, J. Li, B. Liu, et al., ChemSusChem 16 (2023) e202201200.
[28] L. Yang, X. Zhu, S. Xiong, et al., ACS Appl. Mater. Interfaces 8 (2016) 13966–13972.
[29] S. Xiao, J. Zhang, Y. Deng, et al., ACS Appl. Energy Mater. 3 (2020) 4923–4930.
[30] M.S. Bazarjani, M. Hojamberdiev, K. Morita, et al., J. Am. Chem. Soc. 135 (2013) 4467–4475.
[31] F. Xie, M. Xiong, J. Liu, et al., ChemElectroChem 9 (2022) e202200474.
[32] B. Zhang, C. Luo, Y. Deng, et al., Adv. Energy Mater. 10 (2020) 2000091.
[33] S. Wei, M. Serra, S. Mourdikoudis, et al., ACS Appl. Mater. Interfaces 14 (2022) 46386–46400.
[34] S. Dey, K. Manjunath, A. Zak, G. Singh, ACS Omega 8 (2023) 10126–10138.
[35] S. Huang, Y. Wang, J. Hu, et al., ACS Nano 12 (2018) 9504–9512.
[36] H. Lin, L. Yang, X. Jiang, et al., Energy Environ. Sci. 10 (2017) 1476–1486.
[37] J. Jang, S.H. Song, H. Kim, et al., ACS Appl. Mater. Interfaces 13 (2021) 14786–14795.
[38] T. Li, B. Ding, J. Wang, et al., ACS Appl. Mater. Interfaces 12 (2020) 14993–15001.
[39] X. Guan, H. Pei, X. Chen, et al., J. Colloid Interface Sci. 652 (2023) 997–1005.
[40] C. Ding, M. Niu, C. Cassidy, et al., Small 19 (2023) 2301755.
[41] R. Sun, M. Qu, L. Peng, et al., Small 19 (2023) 2302092.
[42] T. Huang, G. Zhang, R. Chen, et al., ACS Appl. Mater. Interfaces 15 (2023) 21075–21085.
[43] X. Zhang, Z. Liu, W. Liu, J. Han, W. Lv, ACS Appl. Mater. Interfaces 15 (2023) 19002–19010.
[44] T. Lei, W. Chen, J. Huang, et al., Adv. Energy Mater. 7 (2017) 1601843.